Next generation neural mass and field modelling

Áine Byrne,[*] Reuben O' Dea[†,*], Michael Forrester[††], James Ross[†‡], and Stephen Coombes[†§]

Abstract

The Wilson–Cowan population model of neural activity has greatly influenced our understanding of the mechanisms for the generation of brain rhythms and the emergence of structured brain activity. As well as the many insights that have been obtained from its mathematical analysis, it is now widely used in the computational neuroscience community for building large scale *in silico* brain networks that can incorporate the increasing amount of knowledge from the Human Connectome Project. Here we consider a neural population model in the spirit of that originally developed by Wilson and Cowan, albeit with the added advantage that it can account for the phenomena of event related synchronisation and de-synchronisation. This *derived* mean field model provides a dynamic description for the evolution of synchrony, as measured by the Kuramoto order parameter, in a large population of quadratic integrate-and-fire model neurons. As in the original Wilson–Cowan framework, the population firing rate is at the heart of our new model; however, in a significant departure from the sigmoidal firing rate function approach, the population firing rate is now obtained as a real-valued function of the complex valued population synchrony measure. To highlight the usefulness of this *next generation* Wilson–Cowan style model we deploy it in a number of neurobiological contexts, providing understanding of the changes in power-spectra observed in EEG/MEG neuroimaging studies of motor-cortex during movement, insights into patterns of functional-connectivity observed during rest and their disruption by transcranial magnetic stimulation, and to describe wave propagation across cortex.

New & Noteworthy: Here we review a new type of neural mass model that is derived from an underlying spiking network with synaptic interactions. This *mean field model* gives a macroscopic dynamical description in terms of a population firing rate and the degree of within-population synchrony. We consider applications to understanding beta-rebound observed in neuroimaging studies during movement, the effects of transcranial magnetic stimulation on functional connectivity networks, and large-scale cortical wave propagation.

---

[*]Center for Neural Science, New York University, New York, NY 10003 USA, and School of Mathematics and Statistics, University College Dublin, Dublin, Ireland. email: aine.byrne@ucd.ie. Orcid ID: 0000-0002-8424-8710

[†]Centre for Mathematical Medicine and Biology, School of Mathematical Sciences, University of Nottingham, Nottingham, NG7 2RD, UK.

[*]email: reuben.odea@nottingham.ac.uk. Orcid ID:0000-0002-1284-9103

[†]email: michael.forrester@nottingham.ac.uk. Orcid ID: 0000-0002-1334-8618

[‡]email: pmxjr3@exmail.nottingham.ac.uk. Orcid ID: 0000-0002-4894-7450

[§]email: stephen.coombes@nottingham.ac.uk. Orcid ID: 0000-0003-1610-7665

1 Introduction

To recognise that the neuroscience community is fascinated with the physiological basis of brain rhythms is an understatement. Indeed, the study and exploration of mechanisms that coordinate such rhythms has generated many interesting discoveries in neuroscience, including their strong correlation with cognitive processing, and that synchrony between brain regions may regulate large scale neuronal communication [37]. A wonderful overview of the 'Rhythms of the Brain' can be found in the book, of the same title, by György Buzsáki [14]. Hand in hand with advances in knowledge gained from cellular, systems, and cognitive neuroscience, has come complimentary work from the theoretical neurosciences. After the Hodgkin–Huxley single neuron model, the population model of Wilson–Cowan is perhaps the most well known [130, 131]. Building on earlier work by Beurle [8] in the 1950s, the 1970s model of Wilson and Cowan developed a theory for neural dynamics to describe populations of interacting excitatory and inhibitory neurons with, or without, refractory states. Moreover, they introduced many ideas from dynamical systems to the wider community, highlighting that switching, cycling, and information storage could all be viewed using the framework of attractor dynamics. For a nice historical perspective on the development of their ideas we highly recommend the interview between Jack Cowan and Edward Rosenfeld that can be found in [4], as well as the paper by Destexhe and Sejnowski [28] that covers some of the many theoretical developments that the Wilson–Cowan model has inspired. Much of the development of Jack Cowan's work in the 1970s took place in the Cummings Life Science Center at the University of Chicago, building on the activity of Nicholas Rashevsky's mathematical biophysics group that included Leon Glass, Stewart Kauffman, and Art Winfree*. Jack Cowan's work tapped into new mathematical results in catastrophe theory [23], dynamical systems [31], and pattern formation [33], and was promoted to the experimental community at events such as the Gordon Research Conferences on Theoretical Biology and Bioinformatics in 1972 and 1973 (with speakers that include other well-known theoreticians such as Wilfrid Rall, John Rinzel, René Thom and Walter Freeman).

The Wilson–Cowan model has now been used in a variety of incarnations: as a single-node description of excitatory-inhibitory population dynamics, as a building block for larger-scale brain network modelling studies, and as the underpinning of spatially-extended models of neural dynamics at the tissue scale. These have provided insights including the understanding of visual hallucinations [13, 32], binocular rivalry [129], travelling cortical waves [97, 129], epilepsy [80, 110], cognitive dynamics of movement [30], *phase-amplitude* coupling [91], and cortical resonant frequencies [68] to name but a few. When considering variants of the Wilson–Cowan model this list expands even further to include the interpretation of neuroimaging data [120], with the most well known of these Wilson–Cowan style models being those of Zetterberg *et al.* [134], Jansen and Rit [57], and Liley *et al.* [71]. Moreover, Wilson–Cowan style neural mass models are a key component of the Virtual Brain project that aims to deliver the first simulation of the human brain based on personalised large-scale connectivity [105].

A core part of the Wilson–Cowan modelling framework is the use of a sigmoid func-

---

*Apparently this was also a great time to play ping-pong on the 9th floor, and many thanks to Bard Ermentrout and John Rinzel for tales of Jack's scientific and ping-pong exploits. The latter covering the gathering of crowds at conferences to watch Jack play Bob May.

tion to determine population firing rates in terms of population activity. Although the use of a sigmoid is now ubiquitous throughout computational neuroscience, in the original Wilson–Cowan model formulation this was assumed to arise via some form of averaging over heterogeneity or noise in networks of simple threshold elements. Thus, although the Wilson–Cowan model can be derived from an underlying microscopic dynamics, this does not come from a biophysically detailed description of a spiking neuron. Nonetheless, in the absence of a general mathematical methodology to develop a statistical neurodynamics from networks of conductance based Hodgkin-Huxley style neurons with chemical synapses, the Wilson–Cowan model has been a hugely popular *phenomenological* model of cortical dynamics.

At the tissue level, the spatially extended Wilson–Cowan model can be conceived of as a (spatially continuous) network of neural masses describing population activity, and is often referred to as a *neural field*. There are now a variety of neural field models, distinguished by the type of neural mass model from which they are constructed. All of them adopt a form of non-local spatial interaction to describe anatomical connections and signalling along axonal fibre tracts. However, all modern neural field models of cortical tissue trace their roots back to the seminal work of Wilson and Cowan [130, 131], recently reviewed in the book 'Neural fields: Theory and Applications' [22], and their mathematical formulation has hardly changed since their original work. Since they describe neural population activity at spatiotemporally coarse-grained scales, they invariably lack important physiological mechanisms known to be fundamental in generating brain rhythms, such as dendritic morphology and nonlinear ionic currents. Nonetheless their basic structure has been shown to provide a mechanistic starting point for understanding whole brain dynamics, and such models form the backbone of many cortical modelling studies.

Given the wealth of neuroscience data now accruing through projects such as the Brain Activity Map in the US, seeking to establish a functional connectome of the entire brain, there is now a community-wide need to develop the next generation of neural mass and field models that have a stronger connection to biological reality. This is especially important when one appreciates that many large scale neuroimaging modalities reflect not only the underlying firing rate of a population of neurons, but also their degree of *synchrony*. A case in point is the well known phenomenon of event related synchrony/de-synchrony (ERS/ERD), as measured by changes in power at given frequencies in electroencephalogram recordings [95]. The neural dynamics underlying ERD and ERS is most likely a manifestation of a spiking network, with enhanced ERS being linked to an increase in the coherence (synchrony) of spike trains. Thus, in view of their coarse-grained natures, neural mass models in isolation are not natural candidates for modelling ERS/ERD; in fact, one cannot model population synchrony with an isolated traditional neural mass model. However, very recent progress in this area has been made for the case of a globally coupled network of quadratic integrate-and-fire (IF) neurons, making use of the Ott-Antonsen ansatz to derive an exact reduced systems of equations (in the thermodynamic limit) [16, 19]. This gives rise to a *neural mass* model with a derived firing rate that is a real function of the complex valued Kuramoto order parameter Z for synchrony, and is therefore a marked departure from the sigmoidal firing rate functions used by Wilson and

Cowan. The relationship between synchrony and rate f takes the explicit form

$$f(Z) = \frac{1}{\pi\tau}\text{Re}\left(\frac{1 - Z^*}{1 + Z^*}\right),\tag{1}$$

where τ is the effective membrane time constant of the neurons and Z^* is the complex conjugate of Z. Here Z is governed by a nonlinear differential equation that couples to the chosen model of the synaptic current. The use of the Kuramoto order parameter in neuroscience is now very prevalent, especially as it relates to the original phase-oscillator network model of Kuramoto [12]. However, its role in neural mass modelling has only recently been realised [65, 76, 84]. The contribution of this paper is to give an introduction to a new class of neural mass and field models that utilise (1), highlighting their benefits to large-scale neuronal population modelling in neuroscience.

In §2–**Neural mass model** we give a full description of the dynamics that accounts for the evolution of synchrony within a prototypical next generation neural mass model, and how this couples to the dynamics of a conductance based model of a synapse. Moreover, we give an interpretation of all parameters and state variables within this mean-field model in terms of the underlying spiking network dynamics from which it is derived. This section effectively introduces a single node description of an excitatory-inhibitory population in the spirit of Wilson and Cowan, that can either be studied in response to stimulation, or used as a building block for large-scale brain network modelling studies. Before turning to the latter, we first consider the usefulness of a single node model in generating power spectrograms of the type commonly found in electro- and magneto-encephalography (EEG/MEG) studies of movement. The model is relevant for understanding the differences in ERD/ERS observed between healthy controls and schizophrenia patients, and a simple extension to a two node model with bi-directional coupling can model the disparities seen between contralateral and ipsilateral hemisphere responses to motor commands. The use of a larger network of such next generation neural masses as an *in silico* testing ground for ideas about the mechanism and control of brain states is explored in §3–**Neural mass network model**. As well as using the model to probe the link between structural and functional connectivity, we also explore the response of networks to stimulation (for networks built using human connectome data). We demonstrate that this has major potential for the design of improved transcranial magnetic stimulation protocols. Moving away from parcellated models of the cortex, we turn, in §4–**Neural field model**, to continuum models of cortical surfaces. Here we illustrate how the relevant neural field models, with realistic patterns of structured axonal interactions, can be viewed in terms of a generalised brain-wave equation of Nunez type [90]. Numerical simulations are used to illustrate the patterns of propagating waves that can be supported, both with and without a form of adaptation that mimics local metabolic processes. Finally in §5–**Discussion** we discuss the future steps for the development and further application of next generation neural mass and field models.

2   Neural mass model

Neural mass models generate brain rhythms using the notion of population firing rates, aiming to side-step the need for large scale simulations of more realistic networks of spiking neurons. Although they are not derived from detailed conductance based models they

can be motivated by a number of phenomenological arguments [22], and typically take the form of systems of nonlinear ordinary differential equations (ODEs). The Wilson–Cowan neural mass model describes the dynamics of two interacting populations of neurons, one of which is excitatory and the other inhibitory. Interactions between the populations are mediated by a nonlinear sigmoidal firing rate function. In its most simple incarnation it consists of two nonlinear ODEs, and as such, has been widely studied using techniques from phase-plane analysis and numerical bifurcation theory. Caricaturing the sigmoid with a piecewise linear function also allows for a more explicit mathematical analysis, including the construction of oscillations and the determination of their stability [20].

Building on work by Luke *et al.* [76], Laing [65], and Montbrió *et al.* [84], recent studies at the intersection of theoretical neuroscience and self-organised systems have led to the formation of a generalised neural mass model [16, 19]. The model takes a similar form to that proposed by Wilson and Cowan in 1972 [130], and for clarity of exposition we first write the model for a population of neurons with global self-feedback through a set of synapses with overall conductance g. This conductance evolves according to the dynamical system

$$Qg = \kappa f(Z), \tag{2}$$

with the firing rate $f(Z)$ given by (1). Here κ is the strength of coupling and the differential operator Q is chosen to best capture the temporal characteristics of synaptic response. For the popular α-function synapse, with shape $\alpha^2 t e^{-\alpha t}$ following the arrival of an action-potential at time $t = 0$, we would choose

$$Q = \left(1 + \frac{1}{\alpha}\frac{\mathrm{d}}{\mathrm{d}t}\right)^2, \tag{3}$$

and see [16] for other choices. The form of equation (2) is common in neural mass modelling, albeit with a different form of closure, whereby $Qg = \kappa f(g)$, with f chosen to be a sigmoidal function. The major modelling departure in the use of equation (2) is that here f is a *derived* quantity and, additionally, it is a function of the dynamic synchrony variable Z, with magnitude R and phase Ψ, so that $Z = Re^{i\Psi}$. Hence, we have a direct link between the within-population synchrony and the synaptic activity. The synchrony variable, known as the Kuramoto order parameter evolves as follows:

$$\tau\frac{\mathrm{d}}{\mathrm{d}t}Z = \mathcal{F}(Z; \eta_0, \Delta) + \mathcal{G}(Z, g; v_{\mathrm{syn}}), \tag{4}$$

where

$$\mathcal{F}(Z; \eta_0, \Delta) = -i\frac{(Z-1)^2}{2} + \frac{(Z+1)^2}{2}\left[-\Delta + i\eta_0\right] \tag{5}$$

$$\mathcal{G}(Z, g; v_{\mathrm{syn}}) = i\frac{(Z+1)^2}{2}v_{\mathrm{syn}}g - \frac{(Z^2-1)}{2}g. \tag{6}$$

To interpret the model parameters Δ, η_0 and v_{syn}, we must examine the underlying spiking model from which it is derived, namely the quadratic integrate-and-fire (QIF) network model. A QIF neuron in a globally coupled synaptic network indexed by $i = 1, \ldots, N$ evolves according to

$$\tau\frac{\mathrm{d}}{\mathrm{d}t}v_i = \eta_i + v_i^2 + g(v_{\mathrm{syn}} - v_i), \qquad Qg = \frac{\kappa}{N}\sum_{j=1}^{N}\sum_{m\in\mathbb{Z}}\delta(t - T_j^m), \tag{7}$$

subject to *reset* $v_i \rightarrow -\infty$ whenever v_i reaches $+\infty$ in finite time and *fires*. These firing events occur at times T_i^m, where m indexes the mth time that neuron i fires. The background drives η_i are chosen from a normalised Lorentzian distribution with center η_0 and width Δ, and v_{syn} corresponds to the synaptic reversal potential of the neurons. Here, the inputs η_i are "quenched", though it is also possible to obtain similar model behaviour (to that reported below) with identical neurons ($\eta_i = \eta_0$ for all i) driven by noise [84]. For a full description of how to derive (2) and (4) from (7) as $N \rightarrow \infty$ see [16, 19]. Thus the mean-field description of a globally coupled QIF network with a shunted synaptic current modelled using an α-function conductance change is given by just four ODEs. Two of these, given by (4), describe the evolution of the complex Kuramoto order parameter for synchrony, and the other two, given by (2), describe how this couples to the dynamics of the synaptic conductance. For simplicity we now set $\tau = 1$ throughout the rest of this paper (unless otherwise stated). Figure 1 demonstrates that the dynamics of the order parameter Z and synaptic conductance g for a simulation of 500 QIF neurons described by (7) (red) and the mean field model, given by (2) and (4) (blue), are closely matched. It is very straightforward to extend the above to treat populations of
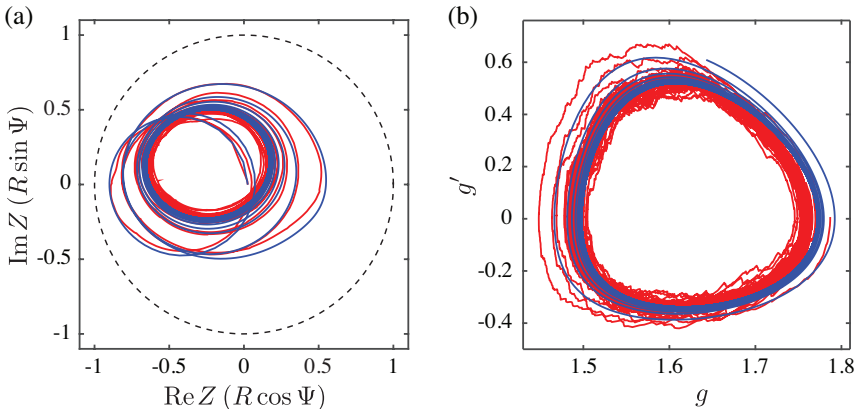

Figure 1. Validation of mean field reduction. Comparison of dynamics for mean field model (blue) (2)–(4) and simulation of 500 coupled QIF neurons (red) (7). (a) Phase plane of the Kuramoto order parameter $Z = Re^{i\Psi}$. (b) Synaptic conductance g vs rate of change of synaptic conductance g'. Parameter values: $\eta_0 = 20$, $\Delta = 0.5$, $v_{\text{syn}} = -10$, $\kappa = 1$, $\alpha = 0.95$.

interacting excitatory and inhibitory neurons. In this case each neuronal population has two types of synaptic conductances associated with it, one to describe inhibition and the other for excitation. If each synapse has a conductance change modelled as an α-function then eight first order ODEs are needed to model the four populations of synapses, with a further four required to model the degree of synchrony in the excitatory and inhibitory neuronal populations respectively. This gives a minimal model of a patch of cortex in terms of twelve first-order ODEs, which can be reduced in number by dropping cross-interactions (such as self-inhibition), and / or choosing a first order differential operator for Q, such as $(1 + \alpha^{-1}\mathrm{d}/\mathrm{d}t)$, describing a *fast* synapse with an exponential decay rate α^{-1}. The form of this minimal model of cortex as a *single* node, encapsulating local

interactions of both excitatory and inhibitory type, is generalised from (2) and (4) as

$$Q_{ab}g_{ab} = \kappa_{ab}f(Z_b), \qquad \tau_a \frac{\mathrm{d}}{\mathrm{d}t}Z_a = \mathcal{F}_a(Z_a; \eta_0^a, \Delta^a) + \sum_b \mathcal{G}(Z_a, g_{ab}; v_{\mathrm{syn}}^{ab}), \qquad (8)$$

where $a, b \in \{E, I\}$ represent labels for excitation (E) and inhibition (I), Q_{ab} is obtained from (3) under the replacement $\alpha \to \alpha_{ab}$ (so that the time course of synaptic responses can differ), and v_{syn}^{ab} is the reversal potential mediating the current from population a to population b.

Neural oscillations, as observed using EEG/MEG, are thought to be the result of neurons synchronising their firing times to create coherent high amplitude oscillations. To better understand these oscillations and how certain tasks can modulate their amplitude, it is important to examine the synchronisation properties of the underlying neurons. Next we explore how the model can be used to explore ERD/ERS and other changes in neural synchrony.

2.1 Beta rebound

Neural activity in the beta-band (13–30 Hz) has long been associated with movement. In particular, execution of a movement results in a decrease of beta power in the motor cortex, termed movement-related beta decrease, (MRBD), followed by an increase above baseline upon movement termination (post-movement beta rebound; PMBR) (Fig. 2(a)). It is hypothesised that this event-related modulation corresponds to changes of synchrony within motor cortex [115]. Given that the neural mass model described above can track within-population synchronisation (and that standard neural mass models cannot), it was deemed an ideal candidate for modelling this phenomena by Byrne *et al.* [16]. Simulating a single inhibitory population with a time dependent drive (2)–(4), the authors linked changes in synaptic activity to changes in the underlying synchronisation (Fig. 2(c) & (d)). In the absence of drive the model oscillated at ~ 15 Hz. When the drive was switched on (movement initiation), the beta-band oscillations disappeared. After the drive was removed (movement termination), the spectral power in the beta-band rebounded above baseline, before it settled back to its original value (Fig. 2(d)). Examining the phase plane of the order parameter Z (Fig. 2(c)), they showed that after the drive is switched off (green curve) the order parameter is attracted to the edge of the unit disc (maximal synchrony $R = 1$) before spiralling back to the original limit cycle.
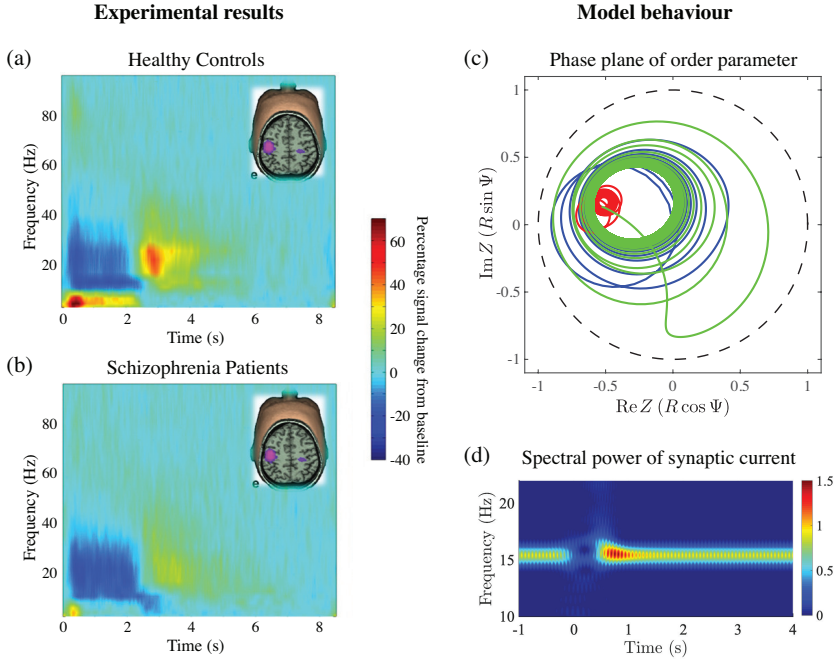
Figure 2. Beta rebound. (a) Time frequency spectrogram showing percentage change from baseline of a trial averaged signal from the motor cortex during a motor task. We see stereotypical movement related beta decrease (MRBD) from $0-2$ s and the post movement beta rebound (PMBR) at roughly 2.5 s. (b) Time frequency spectrograms for schizophrenia patients doing the same task. There is a significant decrease in PMBR. (c) Model results for the Kuramoto order parameter during a simulated movement. Synchrony is maximal along the dashed circle and minimal at the centre of the disk. The red curve shows the behaviour during the simulated movement, while the green corresponds to the time after movement termination. After movement termination there is an increase in synchrony (curve approaches dashed line), before the system returns to its original behaviour. (d) Time frequency spectrogram for the synaptic current, showing qualitatively similar properties to the experimental results in (a). There is a reduction in beta power at movement onset (0 s), followed by a sharp increase in power shortly after movement termination (0.5 s). Parameter values: $\eta_0 = 21.5$, $\Delta = 0.5$, $v_{\text{syn}} = -10$, $\kappa = 0.105$, $\alpha^{-1} = 35$ ms, $\tau = 31$ ms. Data for panel (a) and (b) from [99].

Human MEG studies reveal beta rebound on both sides of the motor cortex during movement. The strongest rebound is seen in the contralateral hemisphere, with a weaker rebound in the ipsilateral hemisphere. Contralateral refers to the side of the brain that sends and receives the motor commands, while the ipsilateral hemisphere receives the input indirectly from the contralateral hemisphere, through bi-lateral coupling. In the above we considered a single node, assumed to represent the contralateral motor cortex. To examine the interplay of the contralateral and ipsilateral hemispheres, we introduce a second identical node. The coupling between the two is bi-directional, with a long synaptic timescale. This two hemisphere model successfully produces MRBD and PMBR in both populations with a larger PMBR in the contralateral (driven) hemisphere (Fig. 3(a)) than the ipsilateral hemisphere (Fig. 3(b)).

The presence of the second population leads to the emergence of co-existing oscilla-
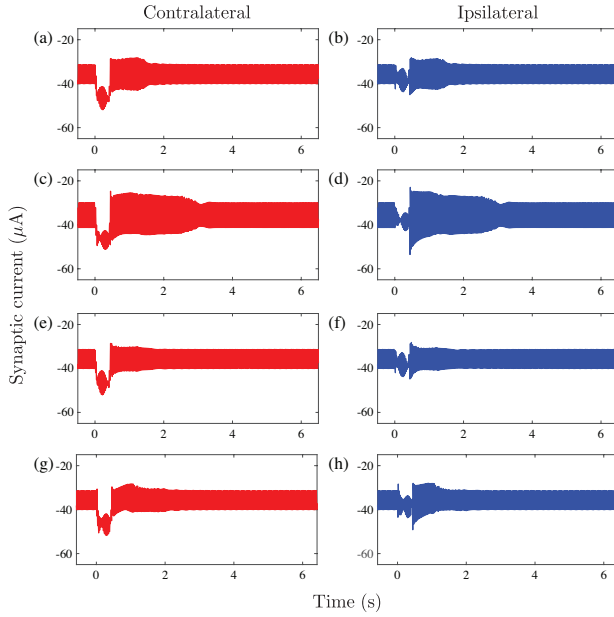
Figure 3. Two hemisphere model. Response of the system to a temporally filtered square pulse of length 0.4 s and magnitude 10 μA. As in experimental findings, the contralateral hemisphere shows a larger rebound than the ipsilateral hemisphere. Different initial conditions were used for each row, resulting in different magnitudes and lengths of the rebound in oscillatory amplitudes. Parameter values: $\eta_0 = 23$, $\Delta = 0.5$, $v_{\text{syn}}^{ii} = -10$, $v_{\text{syn}}^{ij} = -10$, $\kappa_{ii} = 4.5$, $\kappa_{ij} = 5.4$, $\alpha_{ii}^{-1} = 30$ ms, $\alpha_{ij}^{-1} = 75$ ms, $\tau = 30$ ms, were we use ii to denote intra-hemisphere connections and ij for inter-hemisphere connections.

tory solutions, i.e. different initial conditions can lead to different behaviours. Depending on which of the two states the system is in, it will react differently to the motor command. The magnitude and length of PMBR is also heavily dependent on the phase of the oscillation when the drive is applied (Fig. 3(a)-(h)), as well as the oscillatory state it is in. This variability in the model response is akin to MEG recordings, where individual trials show large variability in the magnitude and length of PMBR. It is only upon averaging over many trials that we see the stereotypical MRBD and PMBR, as shown Fig. 2(a).

Beta decrease (MRBD) and rebound (PMBR) are special cases of ERD and ERS, respectively. Event-related changes in synchrony are observed in many different brain areas for a range of different frequencies. By modifying the model parameters, we can change the frequency of oscillation of the population and explore other types of ERS/ERD, such as the attenuation of the alpha rhythm upon eye opening. We emphasise again that standard neural mass models, based on Wilson-Cowan style descriptions, cannot describe ERD/ERS because their level of coarse-graining does not allow one to interrogate the degree of within-population synchrony.

2.2 Beta burst

Recent experimental evidence suggests that beta-band activity is stochastically transient, rather than steady and sustained as previously thought [34, 77]. Electrophysiological recordings, such as EEG and MEG, are typically trial averaged to produce clear time-frequency spectrograms. Transiently occurring bursts of beta activity could present as a sustained rhythm in a trial averaged regime, leading experimentalists to search for these *beta bursts* in single trial EEG and MEG data. At a single-trial level, spontaneous brain activity in motor areas indeed shows transient bursts of beta-band activity lasting $\sim$ 150 ms [108]. When trial-averaged, this same activity appears sustained with a relatively constant power level.

As well as sustained beta oscillations, the model can also support beta bursts when pink noise is added to the system. Using an excitatory-inhibitory pair, and setting the parameter values close to the boundary between oscillatory and stationary behaviour, noise can perturb the system temporarily into the oscillatory state. When the system is perturbed into the oscillatory state, we see bursts of high amplitude activity, lasting $\sim$ 200 ms (Fig. 4(a)). The bursts seen in single simulations occur every few seconds, but when averaged over multiple simulations there is a constant power at roughly 20 Hz consistent with trial averaged data (Fig. 4(b)). Interestingly, the time scale of the noise changes the occurrence of the bursts. If the noise frequency is above alpha-band (8 Hz), there is no effect, but for frequencies lower than $\sim$ 8 Hz the number of bursts decreases with noise frequency. Should beta bursts in electrophysiological recordings be characterised by frequency of occurrence in various situations, this model could be used to explore the types of noise responsible for the bursts.
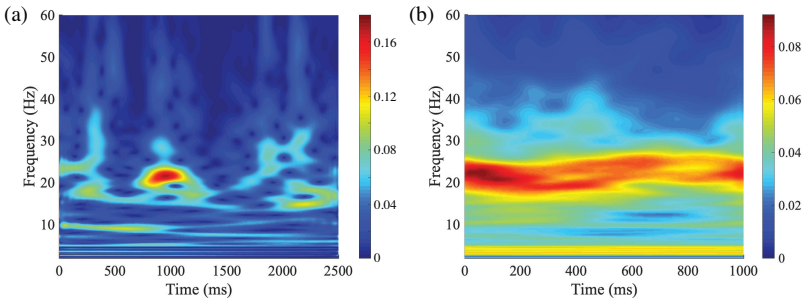

Figure 4. Beta burst. (a) Beta burst in single trial data, (2.5 s simulation). There is a peak peak in beta-band power at roughly 800 ms, lasting $\sim$ 200 ms. (b) Steady beta-band activity in trial averaged data (average spectral power over 20 1 s simulations). Parameter values: $\eta_0^E = 1.6$, $\eta_0^I = 1$, $\Delta_E = 0.2$, $\Delta_I = 0.2$, $v_{syn}^E = 10$, $v_{syn}^I = -12$, $\kappa_{EE} = 1$, $\kappa_{IE} = 1.5$, $\kappa_{EI} = 2$, $\kappa_{II} = 1$, $\alpha_{EE}^{-1} = 3$ ms, $\alpha_{EI}^{-1} = 3$ ms, $\alpha_{IE}^{-1} = 10$ ms, $\alpha_{II}^{-1} = 10$ ms, $\tau_E = 12$ ms, $\tau_I = 18$ ms.

2.3 Neurological disorders

Given the prevalence of EEG/MEG in neuroscience, researchers have begun to ask if these recordings could provide biomarkers for neurological disorders [74]. Abnormal beta oscillations were recently identified as a biomarker of a number of neurological disorders,

such as schizophrenia and Parkinson's disease. Among these abnormalities is a reduction in magnitude of beta rebound. Schizophrenia patients show a similar MRBD, but a reduced PMBR when compared to healthy controls (Fig. 2(a)-(b)), and the severity of the reduction in PMBR is directly correlated to severity of the disease [99]. Byrne *et al.* [17] recently demonstrated that this result could be reproduced using the next generation neural mass model described above with a longer synaptic timescale for the glutamatergic receptor responsible for processing the motor input. This result reaffirms the belief that schizophrenia is an information processing disorder, demonstrating that reducing the synaptic transmission rate reduces the magnitude of PMBR.
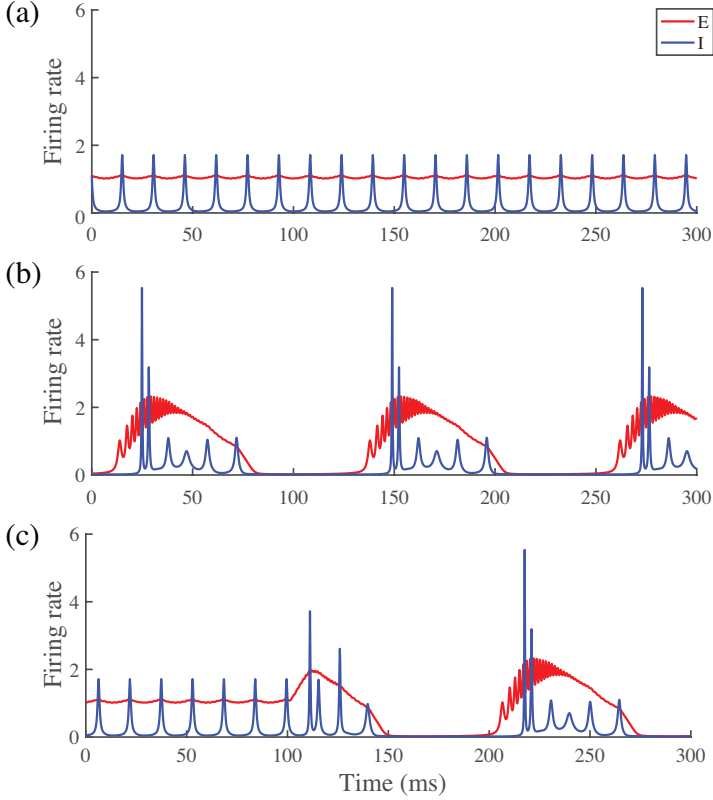

Figure 5. Healthy versus epileptic oscillations. For a large window in parameter space the E-I population model (8) is multi-stable, i.e. different initial conditions can lead to different behaviours, and small perturbations can also lead to a change in behaviour. (a) Regular "healthy" oscillations. (b) Pathological seizure-like oscillations. (c) A small perturbation to the E→E synaptic conductance gives rise to a transition from healthy to pathological behaviour. Parameter values: $\eta_0^E = 10$, $\eta_0^I = 21$, $\Delta_E = 0.5$, $\Delta_I = 0.5$, $v_{\text{syn}}^E = 10$, $v_{\text{syn}}^I = -10$, $\kappa_{EE} = 1.5$, $\kappa_{IE} = 1.5$, $\kappa_{EI} = 4.5$, $\kappa_{II} = 2.4$, $\alpha_{EE}^{-1} = 6.5$ ms, $\alpha_{EI}^{-1} = 20$ ms, $\alpha_{IE}^{-1} = 5$ ms, $\alpha_{II}^{-1} = 7$ ms, $\tau_E = 3$ ms, $\tau_I = 3$ ms.

Recent work on dementia has shown that EEG/MEG power in the delta (< 4 Hz) and theta ($4-7$ Hz) frequency range is notably higher, and alpha ($8-12$ Hz) and beta markedly lower, for dementia patients when compared to normal elderly subjects [6] . In particular,

the dominant oscillatory frequency of the EEG spectrum for dementia patients was found to be lower than for healthy controls [94]. Given that dementia is believed to arise from the deterioration of synaptic connections, the synaptic time scale was increased in order to model these effects. As in the schizophrenia study, increasing the synaptic time scale has the effect of reducing the synaptic efficacy and slowing down signal transfer. In the model, increasing the time scale decreases the population synchrony and in turn the amplitude of the oscillations, for a range of spectral frequencies. The increased synaptic processing time was not enough to decrease the oscillatory frequency, however this decrease may be due to an interplay between the different frequency bands, which was not considered here.

Epilepsy is a neurological disorder characterised by seizures, periods of high amplitude and highly synchronised brain oscillations. Extensive research has been carried out to design treatments and preventative care for epileptic patients. However, the underlying cause of the disorder is still unclear. Previous theoretical studies of epilepsy typically use the Jansen-Rit model [58], as there are parameter windows for which the model can exhibit low amplitude or high amplitude oscillations depending on the initial conditions [2, 43, 119, 128]. However, unlike the model presented here the Jansen-Rit model cannot track neuronal synchrony. The excitatory-inhibitory two population model, given by (8), exhibits multi-stability similar to the Jansen-Rit model. For the same parameter values, the model can exhibit fast low-amplitude oscillations (Fig. 5(a)) or bursts of high-frequency activity at a slow burst rate (Fig. 5(b)). Both states are stable, but perturbations can drive transitions between the states, such as a brief synaptic input to the excitatory population (Fig. 5(c)). Low frequency bursts of high frequency activity (as seen in Fig. 5(b)) are typical of epileptic seizures, providing further evidence that this is a suitable model for theoretical studies of epilepsy. The presence of the synchrony variable should also allow the exploration of how changes in population synchrony can lead to seizures, and help uncover protocols that would lead to seizure termination.

3   Neural mass network model

Advances in non-invasive neuroimaging methods that allow detailed characterisation of the brain's anatomy and activity, together with developments in network science, have supported a proliferation of network connectivity-based approaches, employing neural mass models as building blocks, to understand large-scale brain function. These studies are especially relevant to elucidating the emergence of *functional connectivity* (FC) networks that describe dynamic patterns of temporal coherence of activity between brain regions. Important examples include archetypal brain networks that emerge under different tasks or stimulants [117], and so-called resting state networks [11], whereby different regions of the brain's sensorimotor system oscillate slowly and synchronously in the absence of any explicit task. More generally, these FC networks are posited to support high-level brain function—the divergence between dynamic functional activity and the relatively static structural connections between populations is critical to the brain's wide functional repertoire, and may hold the key to understanding brain activity in health and disease [92, 121, 123]. In particular, disruptions in structural and functional brain networks are linked to a variety of psychiatric and neurological diseases such as epilepsy and schizophrenia [10, 81].

Empirically, FC is typically derived from statistical analyses of time-series data from MEG, EEG, or functional magnetic resonance imaging (fMRI). However, while FC is widely employed in both empirical and theoretical studies, the specific link between the brain's anatomical circuitry and the varied and complex behaviour it exhibits is not fully understood [50, 92]. A plethora of theoretical studies have therefore sought to elucidate SC–FC relationships, employing neural mass models, alongside anatomical connectivity networks, to simulate large-scale brain activity. These investigations have revealed, for example, strong SC–FC correspondence on long time-scales, in comparison to those observed over short time-scales [49, 51, 103] and close resemblance of structural and functional networks when the neural dynamics is near a critical transition [114]. This critical SC–FC correspondence is further highlighted in the work of Hlinka & Coombes [48], using a combination of network graph analysis and dynamical systems theory to expose the role of Hopf bifurcations in the Wilson–Cowan model in organising SC–FC relations; in a similar vein, multiplex clustering measures have also been exploited to emphasise how SC–FC relations vary as a function of Wilson–Cowan model dynamics [24]. These ideas can be further extended to show how the organisation of FC is intrinsically related to the dynamical state of the neural mass system, such that FC patterns can in large parts be understood without recourse to specific connectome information [35, 116].

To develop a large-scale model incorporating interconnected neural populations across the whole brain, we generalise equation (8) to consider N connected populations of excitatory and inhibitory neurons, denoted $E_1, \ldots, E_N$, $I_1, \ldots, I_N$. Therefore, for each network node m we define population order parameters $Z_a \to Z_m^a$ and synaptic conductances $g_{ab} \to g_{ab}^{mn}$ for $a, b \in \{E, I\}$ and $n \in \mathcal{N}(m)$, where $\mathcal{N}(m)$ denotes the set of nodes connected to node m ($n = m$ represents within-node excitatory-inhibitory coupling). We note that since long-range connections in the brain mainly project from excitatory pyramidal cells [41], we restrict inter-mass coupling to connections between excitatory populations. Constants are denoted similarly, with $(\alpha_{ab}, \kappa_{ab}, \eta_0^a, \Delta^a, v_{\text{syn}}^{ab}, \tau_a) \to (\alpha_{ab}^{mn}, \kappa_{ab}^{mn}, \eta_{0,m}^a, \Delta_m^a, v_{mn}^{ab}, \tau_m^a)$. Structural connectivity between neural masses (κ_{ab}^{mn}, $m \neq n$) was estimated from diffusion MRI data from 10 subjects obtained from the Human Connectome Project [122]. Briefly, we explain how this data is post-processed to derive connectomic data, though we direct the reader to [1] (for related work on Wilson-Cowan neural mass networks) and the references therein for a more detailed overview. $60,000$ vertices on the white/grey matter boundary surface for each subject [42] were used as seeds for $10,000$ tractography streamlines. Streamlines were propagated through voxels with up to three fibre orientations, estimated from distortion-corrected data with a deconvolution model [59, 112], using the FSL package. The number of streamlines intersecting each vertex on the boundary layer was measured and normalised by the total number of valid streamlines. This resulted in a $60,000$ node structural matrix, which was further parcellated using the 68-node Desikan-Killiany atlas [26] (note that since each brain region is on the scale of millions of neurons, they are each suitably modelled by a single neural mass). Each element of the connectivity matrix κ_{ab}^{mn} ($m \neq n$) therefore reflects the proportion of white matter fibres which bridge regions m and n.

Functional connectivity is obtained by direct simulation of this neural mass network, and computing the pairwise synchronisation between time-series activity on each network node, measured via the mean phase coherence (MPC; see, *e.g.* [85]), to provide a matrix

describing the strength of functional connection between each brain region. Structure–function relations are assessed by computing the Jaccard similarity coefficient [56] of the non-diagonal entries of the binarised SC and FC matrices, which provides a natural measure of matrix overlap, ranging from 0 for matrices with no common links to 1 for identical matrices.

Results visualising both the structural and derived function networks are shown in Fig. 6; these show how FC patterns can differ significantly from the underlying connectome structure that supports neural population activity. In the following, we describe how the model and approaches described above can be employed to understand the influence of brain stimulation treatments on network behaviour.
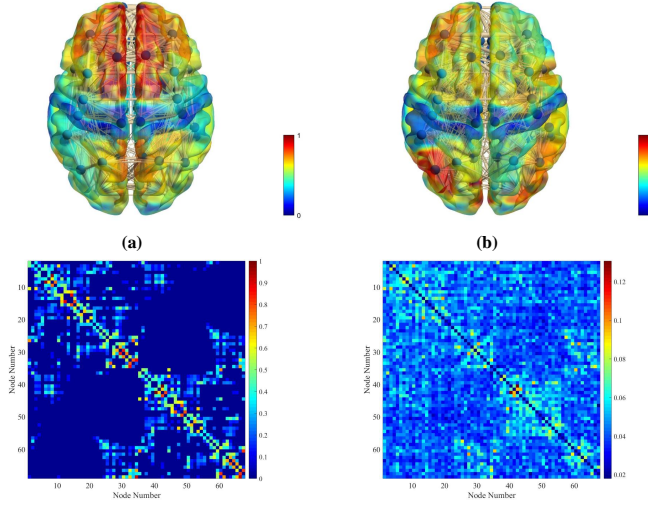

Figure 6. Visual representation of (a) structural network and (b) simulated functional network for 68 nodes parcellated according to the Desikan-Killiany atlas. The surface of the brain visualisations are coloured depending on nodal degree, which was normalised by the highest element for easier comparison between SC and FC. The upper surface plots highlight the strong differences between SC and FC patterns. The network graphs are shown on the bottom row. Parameter values: $\alpha_{EE}^{mn} = 1$, $\alpha_{IE}^{mn} = 1.4$, $\alpha_{EI}^{mn} = 0.7$, $\alpha_{II}^{mn} = 0.4$, $\kappa_{EE}^{mn} = 1.5$, $\kappa_{IE}^{nn} = 1$, $\kappa_{EI}^{nn} = 2$, $\kappa_{II}^{nn} = 3$, $v_{EE} = 10$, $v_{mn}^{IE} = 8$, $v_{mn}^{EI} = -8$, $v_{\text{syn},mn}^{II} = -12$, $\Delta_m^E = 0.5$, $\Delta_m^I = 0.5$, $\eta_{0,m}^I = -20$, $\eta_{0,m}^E = 20$, $\tau_m^a = 1$; values of κ_{EE}^{mn} are obtained from MRI data (see text), scaled by a global coupling strength $\varepsilon = 0.025$.

3.1 Transcranial magnetic stimulation

Transcranial Magnetic Stimulation (TMS) is a non-invasive therapeutic brain stimulation technique whereby strong electromagnetic fields are used to induce a transient current pulse in the brain, in order to influence neural activity, particularly in superficial regions of cerebral cortex. TMS has potentially wide-reaching consequences for mental health conditions, having provided positive outcomes for patients with Parkinson's disease [9, 109], schizophrenia [69, 70] and depression [36, 39, 63, 73]. Though its efficacy in treating these conditions, in some cases, is evidential, the precise neurological effects of TMS

are not understood. Previous studies highlight that TMS can influence neural activity within populations in a range of ways. Initial synchronous depolarisation, followed by longer-lasting GABAergic inhibition [111] impacts on neuronal excitability [67] and the excitatory/inhibitory balance [55], can drive neural plasticity [38], and alter patterns of coherence between brain regions, leading to the reorganisation of functional connectivity networks [55, 118]. Limbic structures have been identified as a critical component of the pathophysiology of depression (see, *e.g.*, [44, 54, 79]), and in particular, the insula is a key part of abnormalities in [5, 53, 72], and interactions between [79, 82, 113] functional networks implicated in depression. However, since TMS induces current on surface regions, sub-cortical regions such as the insula must be influenced indirectly [55]; the mechanisms by which this occurs, and ideal stimulation protocols to achieve this remain unclear. Neural mass models — and, through its account of within-population synchrony, the next-generation neural mass model described herein — are particularly suited to providing an understanding of how such emergent FC patterns can be influenced by TMS, and interrogating the influence of TMS protocols *in silico*, to inform more effective treatment.

TMS pulses begin with a sharp peak to induce an electric field across the cortex, causing electric currents to be generated across cell membranes. This is followed by a slow dissipation, resulting in a much weaker electric field in the opposite direction [101]. Pulses may be delivered as singular bursts, or in high-frequency trains referred to as repetitive TMS (rTMS). Pulses are accommodated in our neural mass network model by modulating the average population drive on each node (see equation (8)): $\eta_0^a \to \eta_{0,m}^a + H_m^a(t)$, and where $a \in \{E, I\}$ and $m \in \{1, \ldots, N\}$, where the function $H_m^a(t)$ is chosen to reflect the particular delivery protocol. For simplicity, in the following we assume that the induced drive is identical for both inhibitory and excitatory populations, with each pulse given by a damped sinusoid:

$$H_m^a(t) = I_{\text{peak}} \sin(\omega(t - t_i))\exp((t_i - t)/\tau)\Theta(t - t_i)\delta_{m,M}, \qquad (9)$$

where M indicates which node (or set of nodes) is stimulated, t_i denotes pulse times, Θ the Heaviside function, $I_{\text{peak}} = 100$ is the pulse amplitude (in arbitrary units), $\omega = 20\text{rad/ms}$ is the wave frequency and $\tau = 0.08$ ms characterises the pulse decay time [104].

To highlight the utility of this approach to understanding the influence of TMS on brain function, we stimulated in turn each of the 14 nodes corresponding to cortical brain regions, and computed the resulting FC network from simulated time-series activity on each node (as described above), paying particular attention to the influence on the right anterior insula. In each case, we employed an rTMS stimulation protocol at 20 Hz [40]. TMS was applied for 50 seconds; functional connectivity was computed after a delay of 50 seconds post-TMS. We note that the stimulation and measurement protocol adopted here was chosen for illustrative purposes rather than to mimic a TMS experiment, allowing for computational efficiency and to allow for transient network activity to decay.

Figures 7 and 8 summarise our results. Fig. 7 shows a representation of the functional network arising from stimulation of each cortical node, interpolated onto brain meshes of the right hemisphere, together with the node corresponding to the insula (right hemisphere). Here, the weighted degree of each node in the FC graph was calculated and
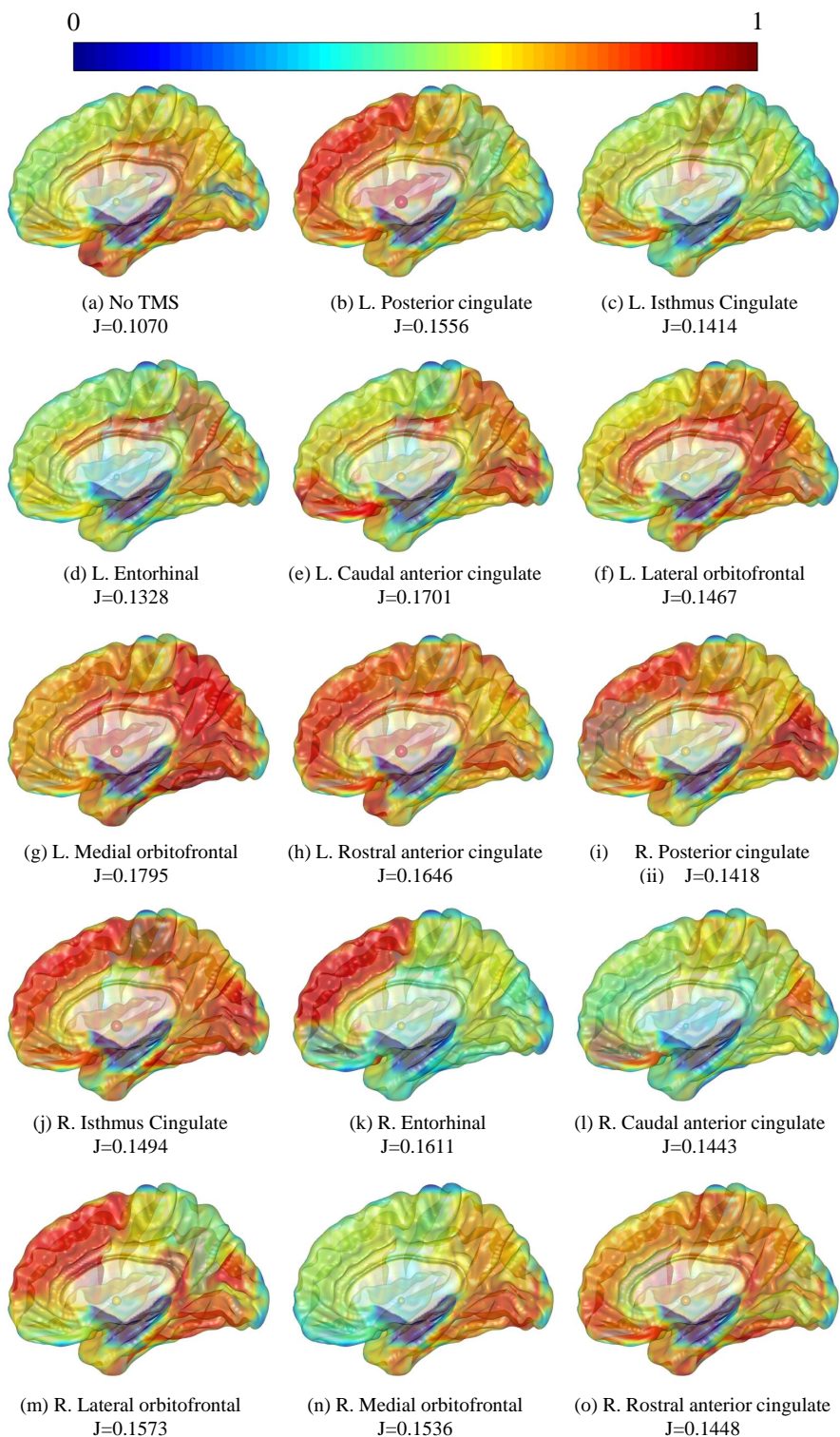
Figure 7. Normalised node degree of FC networks under rTMS stimulation of each cortical area. FC matrices are interpolated on brain meshes of the right hemisphere. The node representing the right anterior insula is also shown to depict the relative influence on stimulation of nodes on a specific sub-cortical region. Figures created with BrainNet Viewer [133]. Parameters as in Fig. 6.

normalised by highest degree. The global SC–FC similarity (measured by the Jaccard similarity coefficient) is also shown. These results highlight the dramatic difference that stimulating each cortical site can make to both the overall pattern of functional connectivity, and the resulting influence on the insula, in particular. This is explored in more detail in Fig. 8, which shows the influence of each stimulated region on some exemplar graph-theoretical properties, as discussed in [88, 102], of the insula node (specifically, the node degree, eigencentrality and clustering coefficient), together with the path-length between the stimulation site and the insula. These results reemphasise the strong dependence of emergent FC on stimulation site indicated in Fig. 7, both in terms of global SC–FC similarity, and specific influence on the insula. Moreover, the efficacy of stimulation is not strongly predicted by proximity (as measured by shortest path length connecting the stimulation site, and the insula), highlighting a non-trivial dependence on macroscopic brain network architecture.
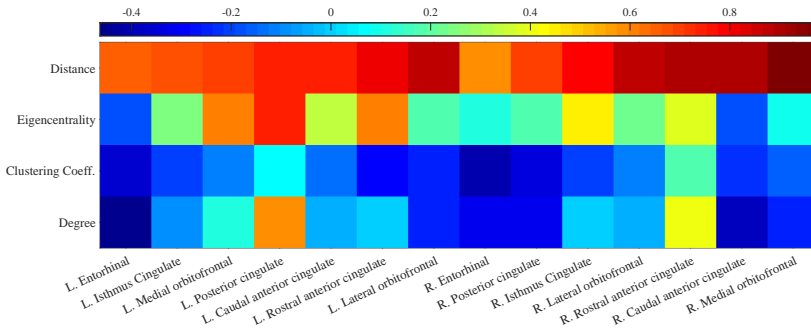

Figure 8. Graph properties of the right anterior insula in FC networks obtained under rTMS stimulation of each cortical area. Shown is: the shortest path length between the stimulated area and the right anterior insula; and the eigencentrality, clustering coefficient, and node degree of the insula node. Parameters as in Fig. 7.

We have shown results from a range of target regions to show the variability of simulated TMS-induced FC states. However, more clinically relevant TMS protocols could be implemented such as stimulation of the dorsolateral prefrontal cortex, which has frequently been the subject of TMS studies related to the treatment of major depression [66, 89].

4 Neural field model

The structure of the neocortex is well known to have a columnar organisation [86], built from macrocolumns of $\sim 10^6$ neurons with similar response properties, and that these tend to be vertically aligned into columnar arrangements of roughly $1 - 3$ mm in diameter. Intracortical connections can range over $1 - 15$ cm, allowing communication between distal cortical areas. Thus it is natural to view the human cortex as a dense reciprocally interconnected network of roughly 10^{10} corticocortical axonal pathways that make connections within the roughly 3 mm outer layer of the cerebrum [45]. Given the shallow

depth of this wrinkled and folded cortical structure with a high neuronal density, it is common from a modelling perspective to use a *neural field* description (not to be confused with the neural mass model described earlier). This is essentially a coarse grained description of neural tissue that describes the evolution of neuronal activity on a two dimensional surface, although theoretical analyses of such models are often carried out just considering one spatial dimension for simplicity. See [22] for an overview. These models can incorporate large scale anatomical knowledge, including the fact that most long-range synaptic interactions are excitatory, with excitatory pyramidal cells sending their myelinated axons to other parts of the cortex. Inhibitory interactions, on the other hand, tend to be much more short-ranged. For excitatory connections it is now known that the weight of connection between two areas decays exponentially with their wiring distance, with a characteristic distance of ~ 11mm (see [127] for a recent discussion). It is the combination of *local* synaptic activity (seen in the rise and decay of post synaptic potentials with time-scales from $1 - 100$ ms) and *non-local* delayed interactions within the cortex (of up to 30 ms in humans) that is believed to be the major source of large-scale EEG and MEG signals recorded at (or near) the scalp. Nunez, in particular, [64] has emphasised the important role that delays arising from action potential propagation along corticocortical fibres have in generating brain rhythms seen in the $1 - 15$ Hz range. Moreover, he has proposed a damped inhomogenous *brain-wave* equation describing the evolution of neural activity at the tissue level that has played an important role in our understanding of waves and patterns seen using EEG sensors [64, 90]. A recent study of the Nunez model on a sphere can be found in [125], which includes an analysis of both standing and rotating waves.

Here we describe a neural field model that generalises the basic neural mass model given by (2) and (4) to include both the spatial extent of anatomical interactions and the axonal delays that arise. Symbolically we write this in the form $Qg = \psi$, $\psi = w \otimes f(Z)$, where Q and Z are given as before, though here $(g, Z) = (g(\mathbf{r}, t), Z(\mathbf{r}, t))$, where $\mathbf{r}$ indicates a position within the cortical surface (and for simplicity this is treated as a sheet with no depth). The symbol $\otimes$ is used to describe spatial interaction within the neural field model, whilst w represents structural connectivity. For example for an idealised one dimensional setting with $\mathbf{r} = x \in \mathbb{R}$ then we might consider

$$[w \otimes f(Z)](x, t) = \int_{\mathbb{R}} \mathrm{d}y \, w(|x - y|) f \circ Z(y, t - |x - y|/v). \tag{10}$$

Here the anatomical connectivity is described by the distance dependent function w, and axonal transmission delays are prescribed solely in terms of this distance and a uniform axonal speed v. If the former has the normalised exponential dependence $w(x) = \exp(-|x|/\sigma)/(2\sigma)$ then there is an equivalent partial differential equation [60]

$$\left[\left(\frac{1}{\sigma} + \frac{1}{v} \frac{\partial}{\partial t} \right)^2 - \frac{\partial^2}{\partial x^2} \right] \psi = \frac{1}{\sigma} \left(\frac{1}{\sigma} + \frac{1}{v} \frac{\partial}{\partial t} \right) f \circ Z. \tag{11}$$

The only difference between (11) and the original brain wave equation of Nunez [90] is that here f is given by (1). The Nunez model of EEG respects the physiology and anatomy described above and has been particularly successful for describing standing EEG waves that arise by interference in a system with periodic boundary conditions.

In a planar system with a rotationally symmetric anatomical connectivity described by $w(r) = \exp(-r/\sigma)/(2\pi\sigma^2)$ the corresponding brain wave equation is

$$\left[\left(\frac{1}{\sigma} + \frac{1}{v} \frac{\partial}{\partial t} \right)^2 - \frac{3}{2} \nabla^2 \right] \psi = \frac{1}{\sigma^2} f \circ Z. \tag{12}$$

Unlike (11), the wave equation given by (12) is only strictly valid for describing *long-wavelength* solutions. In general we can avoid the assumptions that go into using brain wave equations by working directly with the integral form of ψ. This can be posed on a realistic cortical surface Ω and written as

$$\psi(\mathbf{r}, t) = \int_\Omega d\mathbf{r}' W(\mathbf{r}, \mathbf{r}') f \circ Z(\mathbf{r}', t - \tau(\mathbf{r}, \mathbf{r}')), \tag{13}$$

where the kernels W and τ allow for more general structural and delayed interactions.

In the above discussion we have only considered long range interactions that are excitatory. However, in real cortical tissue metabolic processes would act to limit sustained high firing rates. A simple model of such so-called *spike frequency adaptation* can be developed by replacing the mean drive η_0 by $\eta_0 - \delta a$, for some positive strength of feedback $\delta > 0$ coupled to an adaptation field a. This in turn is driven by the firing rate of the tissue:

$$\tau_A \frac{\partial a}{\partial t} = f \circ Z - a. \tag{14}$$

This form of feedback can also be interpreted as a form of localised synaptic inhibitory feedback. In terms of its effect on a travelling wave the main action of this feedback would be to turn an otherwise travelling front into a travelling pulse of neural activity. A recent analysis of one-dimensional models of the type prescribed by (10) in the absence of axonal delays and adaptation has been given in [15]. In this paper it was shown that the model supports a Turing instability (of a homogeneous steady state), that can lead to the formation of travelling waves, with properties not seen in standard neural field models. The main one being the dynamic evolution of population synchrony within travelling fronts and pulses, as typically seen in networks of spiking neurons. We now turn to the use of the above models, with axonal delays and adaptation, in interpreting and understanding the dynamics of cortical waves as observed in neuroimaging studies. However, it is well to note that other reductions of spiking (linear IF) networks to neural field models are also possible, typically assuming a 'balance' of excitation and inhibition, that can also give a better account of network dynamics than phenomenological neural field models, and see e.g. [96, 100].

4.1 Cortical wave simulations

Travelling waves at the scale of the whole brain have been studied ever since the advent of EEG, with more recent studies progressing with the use of electrocorticography (ECoG), in which arrays of electrodes are placed directly on the cortical surface. Both EEG and ECoG indicate that wave speeds are typically in the $1 - 10$ m/s range (consistent with the axonal conduction speeds of myelinated cortical white matter fibres). The development of multi-electrode array and voltage-sensitive dye imaging techniques has brought us even more information about their spatio-temporal properties and shown that they are present
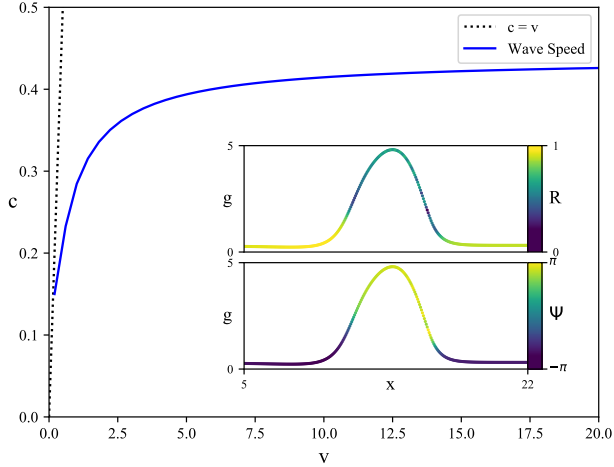
Figure 9. The speed of a travelling pulse in a one dimensional spatial model. The main plot shows the wave speed as a function of the axonal velocity v, highlighting that causality is enforced so that $v < c$, as expected. The figure also highlights that for large v the wave-speed saturates. The insets show a spatial profile for $g = g(x, t)$ at some fixed time t. Encoded on top of this are the values of R and Ψ, where $Z = Re^{i\Psi}$, showing how the degree of synchrony R can vary quite rapidly within a pulse, whilst the phase Ψ switches from just greater than $-\pi$ outside a pulse to roughly π within a pulse. Parameter values: $v = 5$, $\sigma = 1$, $\eta_0 = -3$, $\Delta = 0.5$, $v_{\text{syn}} = 5$, $\kappa = 5$, $\tau_A = 30$, $\alpha = 1$, and $\delta = 5$.

during almost every type of cortical processing [132]. Waves can occur during both awake and sleep states, and can range over both small and large cortical spatial scales. Moreover, they can also occur during pathological states, such as seizures and spreading depression. For a recent discussion of the mechanisms underlying cortical wave propagation, as well as their role in computation, see [87].

The treatment of macroscopic cortical waves is best studied from a theoretical perspective with a wave equation describing the evolution of neural activity at the tissue level. The next generation brain-wave equations given by (11) and (12) are ideal candidates. Here we present simulations of both of these coupled to the adaptation field described by (14), with a focus on the speed and shape of localised travelling solutions. In one spatial dimension we use equation (11) to study a travelling wave of activity. Figure 9 shows that the pulse speed increases linearly with axonal speed v for very small v, and then saturates to a constant value relatively quickly. The shape of the wave is a localised pulse in the conductance variable g, with interesting substructures in the order parameter $Z = Re^{i\Psi}$ within a pulse. The two insets show the variation of R (the degree of synchrony) and Ψ (its phase) across the wave pulse.

In two spatial dimensions we instead use equation (12), and in this case expect to see the radially symmetric counterpart of a travelling pulse in the form of a spreading circular ring, reminiscent of an ictal wavefront [106], as shown in Fig. 10. This is initiated by a localised and transient external input. The internal dynamics for Z within a radial cross

section through the ring of activity shown is reminiscent of that seen in a one dimensional travelling pulse.
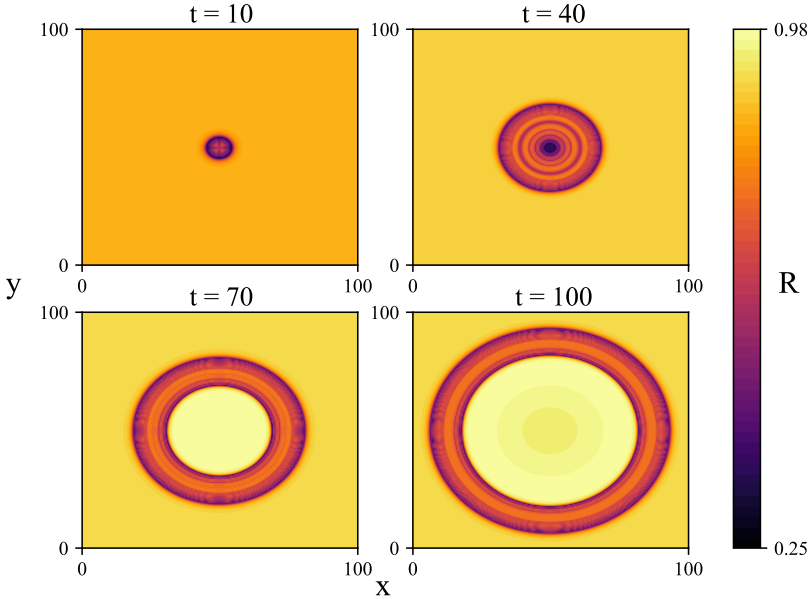

Figure 10. The spread of a travelling ring in a two dimensional spatial model. The images show the magnitude of the synchrony order parameter $|Z| = R(\mathbf{r}, t)$ for different values of time t, with $\mathbf{r} = (x, y)$. The wave is initiated with a localised spatial pulse input in the centre of a planar domain. Parameter values: $v = 10$, $\sigma = 1$, $\eta_0 = -3$, $\Delta = 0.5$, $v_{\mathrm{syn}} = 5$, $\kappa = 5$, $\tau_A = 30$, $\alpha = 1$, and $\delta = 15$.

In many neuroimaging studies of brain waves, authors have reported interesting phase relationships across cortical domains. For example, Alexander *et al.* [3] have observed travelling phase waves at the level of the whole head using MEG (during an observer-triggered apparent motion task), and Denker *et al.* [25] have used multi-electrode arrays to quantify planar, synchronised, random, circular, and radial phase patterns in monkey primary motor cortex. The establishment of phase relationships necessarily requires local oscillations. These can be achieved within the modelling framework presented here in one of two natural ways. The first exploits the fact that in known parameter regimes the point neural mass model can oscillate, either via a Hopf bifurcation or through an isola of limit-cycles [19]. The second utilises the fact that even for standard neural field models with axonal delays that a mixture of short range inhibition and long range excitation can lead to a *dynamic Turing instability* underlying the formation of periodic travelling waves [21]. These generate a phase-relationship between oscillations at different points in the cortical tissue. This second mechanism requires the coupling of brain wave equations, one for each type of synaptic conductance mediating the interaction between excitatory and inhibitory populations (using the population indexing of the mass models as typified by equation (8)), though for brevity we shall not pursue this further here.

5   Discussion

In the last 50 years there has been an active take-up of modelling approaches in the neurosciences, with many of these inspired by the research activity of Jack Cowan. The next generation neural activity models and their application presented here are a case in point, and can trace their scientific roots back to the Wilson–Cowan model. In the spirit of the original Wilson–Cowan model we have reviewed a recent neural mass model for describing the population activity of mesoscopic collections of neurons, and its extension to macroscopic large-scale networks, both discrete and continuum. The local model is ideally suited to studying phenomenon such as event related synchrony/de-synchrony, the discrete network can naturally address the link between structural and functional connectivity, and the continuum model is suited to understanding the properties of cortical wave propagation. In contrast to the Wilson-Cowan model, the one considered here can be derived from an underlying microscopic description of a spiking cell. Admittedly, this is for a specific choice of idealised quadratic integrate-and-fire model, for which the mathematical Ott-Antonsen reduction holds. However, as a common choice for a model of a cortical cell (given its ability to fire at low rate) this is a fortuitous circumstance. Although the search for other mean-field models linked to different choices of single neuron model is of deep mathematical interest, there is clearly a lot of mileage yet to be had in the study and application of the next generation models presented here. It is well to mention a few of these possibilities below.

The first application considered in this paper was to post-movement beta rebound and movement related beta decrease. For simplicity we assumed that these were both mediated by the same type of synaptic receptor. However, Hall *et al*. suggest that movement related beta decrease is a GABA-A mediated process, whilst post-movement beta rebound appears to be generated by a non-GABA-A receptor mediated process [46]. A further model that distinguishes between receptors, may offer important insights into motor processes, and can be readily accommodated within the framework that we have presented here. In the simple two node hemisphere model, the magnitude and length of beta rebound was heavily dependent on the oscillatory phase at which the motor command was applied. This trial-by-trial variability is also true of MEG recording for beta-rebound. Current analysis techniques often remove phase information from recorded MEG activity. However, it is possible to extract this information and test if there is a correlation between the phase of the beta oscillations and the magnitude/length of beta rebound, on a trial-by-trial basis. The phase coherence between the right and left hemispheres would also be an interesting measure to test for correlations. Furthermore, for the beta rebound study we have focused on simple networks built from one or a few nodes, and another intriguing study would would be to explore the spread of beta rebound processes across the cortex, using the neural field formulation.

The second application focused on the use of a neural mass network model (incorporating human connectome data) to relate structural and functional connectivity, and the subsequent use of the same network framework to understand the influence of transcranial magnetic stimulation (TMS) on brain dynamics. This modelling approach would also seem relevant to developing an understanding of treatments for Parkinson's disease. This is a neurodegenerative disorder characterised by excessive synchronisation in the basal ganglia. Deep brain stimulation, the most common surgical intervention for treat-

ing Parkinson's disease, acts to disrupt the high levels of synchrony in the basal ganglia by administering brief pulses of electrical current through the implanted electrodes. This has proven exceptionally powerful in treating the symptoms of Parkinson's disease, yet its success remains poorly understood [107]. Understanding how electrical pulses can disrupt population synchrony and maintain the basal ganglia in an asynchronous state could prove essential for fine tuning deep brain stimulation protocols and providing more effective treatments to Parkinson's patients. Given the ability of the model to track within-population synchrony in a tractable way, it is an ideal candidate for a theoretical study of deep brain stimulation. Similarly there is much further work to be done on using the network model to gain further insight into the effectiveness of transcranial magnetic stimulation protocols in influencing neural states, especially as regards transient neurodisruption [111] and state-dependent effects [93]. Moreover, in this regard it is especially important to consider the development of a sub-cortical model of the thalamus, and the inclusion of thalamocortical connectivity. From a modelling perspective this would require a description of some of the important nonlinear ionic currents known to shape the firing pattern of thalamocortical relay cells and reticular cells [27]. A neural mass that incorporates one such important current, the slow T-type Calcium current, has previously been developed in [18], and next steps could involve a hybrid network that couples this with the next generation model presented here.

The third and final application considered was to whole brain dynamics, and specifically to cortical waves using a generalisation of the brain-wave equation. The study of waves, their initiation, and their interactions is especially pertinent to the study of epileptic brain seizures. However, it is known that gap junctions are especially important in this instance [78], and an important extension of the work presented here is their inclusion in the modelling framework. Laing [65] has already made major inroads on this challenge, and it would be extremely interesting to pursue the translation of this theoretical work to understand how gap junctions may contribute to the generation of spatio-temporal neural rhythms, both functional [7, 52] and pathological [29, 124].

Finally, it is well to mention that the work presented here has ignored any form of plasticity [135], and this almost certainly has an impact on general aspects of brain dynamics such as synchronisation and travelling waves [75], and more specifically on the extensions mentioned above that concern the brain response to transcranial magnetic stimulation and the network dynamics that arise in epilepsy. Given that the next generation model presented here incorporates a conductance based model of the synapse (with reversal potential and bi-exponential temporal response) this can be modulated in a meaningful way to describe various forms of plasticity. As well as incorporating long-term plasticity, say following the route by Robinson for Wilson-Cowan models [98] (and already realised for its importance in transcranial magnetic stimulation [38]), it is also possible to augment the model to treat homeostatic plasticity as advocated by [47, 126] and already implemented in [1] for Wilson-Cowan models. Short-term plasticity has previously been incorporated into neural field models by several authors, mainly through a simple facilitation/depression description as in [61, 62, 83], and can also be naturally included in future studies.

Acknowledgements

References

1. **Abeysuriya RG, Hadida J, Sotiropoulos SN, Jbabdi S, Becker R, Hunt BA, Brookes MJ, Woolrich MW**. A biophysical model of dynamic balancing of excitation and inhibition in fast oscillatory large-scale networks. *PLoS Computational Biology* 14: e1006007, 2018.

2. **Ahmadizadeh S, Karoly PJ, Nešić D, Grayden DB, Cook MJ, Soudry D, Freestone DR**. Bifurcation analysis of two coupled Jansen-Rit neural mass models. *PLOS ONE* 13: e0192842, 2018.

3. **Alexander DM, Nikolaev AR, Jurica P, Zvyagintsev M, Mathiak K, van Leeuwen C**. Global neuromagnetic cortical fields have non-zero velocity. *PLOS ONE* 11: 1–29, 2016.

4. **Anderson JA, Rosenfeld E** 1998 *Talking Nets: An oral history of neural networks*, chapter Jack D Cowan MIT Press, Cambridge, Massachusetts.

5. **Avery JA, Drevets WC, Moseman SE, Bodurka J, Barcalow JC, Simmons WK**. Major depressive disorder is associated with abnormal interoceptive activity and functional connectivity in the insula. *Biological Psychiatry* 76: 258–266, 2014.

6. **Babiloniab C, Percioc CD, Lizio R, Noce G, Cordone S, Lopez S, Soricelli A, Ferrie R, Pascarellie MT, Nobili F, Arnaldi D, Aarsland D, Orzi F, Buttinelli C, Giubile F, Onofrj M, Stocchi F, Stirpe P, Bonanni L**. Abnormalities of cortical neural synchronization mechanisms in patients with dementia due to Alzheimer's and Lewy body diseases: an EEG study. *Neurobiology of Aging* 55: 143–158, 2017.

7. **Bennet MVL, Zukin RS**. Electrical coupling and neuronal synchronization in the mammalian brain. *Neuron* 41: 495–511, 2004.

8. **Beurle RL**. Properties of a mass of cells capable of regenerating pulses. *Philosophical Transactions of the Royal Society London B* 240: 55–94, 1956.

9. **Boggio PS, Fregni F, Bermpohl F, Mansur CG, Rosa M, Rumi DO, Barbosa ER, Odebrecht Rosa M, Pascual-Leone A, Rigonatti SP et al.** Effect of repetitive TMS and fluoxetine on cognitive function in patients with parkinson's disease and concurrent depression. *Movement disorders: official journal of the Movement Disorder Society* 20: 1178–1184, 2005.

10. **Braun U, Muldoon SF, Bassett DS**. On human brain networks in health and disease. *eLS* p. 1–9, 2015.

11. **Breakspear M**. Dynamic models of large-scale brain activity. *Nature Neuroscience* 20: 340–352, 2017.

12. **Breakspear M, Heitmann S, Daffertshofer A**. Generative models of cortical oscillations: Neurobiological implications of the Kuramoto model. *Frontiers in Human Neuroscience* 4: 190, 2010.

13. **Bressloff PC, Cowan JD, Golubitsky M, Thomas PJ, Wiener MC**. Geometric visual hallucinations, Euclidean symmetry and the functional architecture of striate cortex. *Philosophical Transactions of the Royal Society of London. Series B,: Biological Sciences* 356: 299–330, 2001.

14. **Buzsáki G** *Rhythms of the Brain* Oxford University Press, 2011.

15. **Byrne A, Avitabile D, Coombes S**. A next generation neural field model: The evolution of synchrony within patterns and waves. *Physical Review E* 99: 012313, 2019.

16. **Byrne A, Brookes MJ, Coombes S**. A mean field model for movement induced changes in the beta rhythm. *Journal of Computational Neuroscience* 43: 143–158, 2017.

17. **Byrne A, Coombes S, Liddle PF** 2019 *Handbook of Multi-scale Models of Brain Disorders*, chapter A neural mass model for abnormal beta-rebound in schizophrenia Springer.

18. **Coombes S**. Dynamics of synaptically coupled integrate-and-fire-or-burst neurons. *Physical Review E* 67: 041910, 2003.

19. **Coombes S, Byrne A** 2019 *Lecture Notes Nonlinear Dynamics in Computational Neuroscience: from Physics and Biology to ICT*, chapter Next generation neural mass models, p. 1–16 PoliTO. Springer.

20. **Coombes S, Lai YM, Sayli M, Thul R**. Networks of piecewise linear neural mass models. *European Journal of Applied Mathematics* 29: 869–890, 2018.

21. **Coombes S, Venkov NA, Shiau L, Bojak I, Liley DTJ, Laing CR**. Modeling electrocortical activity through improved local approximations of integral neural field equations. *Physical Review E* 76: 051901–8, 2007.

22. **Coombes S, Beim Graben PP, Potthast R, Wright J** *Neural fields : Theory and Applications* Springer, 2014.

23. **Cowan JD, Ermentrout GB** 1978 *Mathematics in Biology*, chapter The eigenbehavior of neural nets Mathematical Association of America, Washington DC.

24. **Crofts JJ, Forrester M, O'Dea RD**. Structure-function clustering in multiplex brain networks. *EPL (Europhysics Letters)* 116: 18003, 2016.

25. **Denker M, Zehl L, Kilavik BE, Diesmann M, Brochier T, Riehle A, Grün S**. LFP beta amplitude is linked to mesoscopic spatio-temporal phase patterns. *Scientific Reports* 8: 5200, 2018.

26. **Desikan RS, Ségonne F, Fischl B, Quinn BT, Dickerson BC, Blacker D, Buckner RL, Dale AM, Maguire RP, Hyman BT et al.** An automated labeling system for subdividing the human cerebral cortex on mri scans into gyral based regions of interest. *NeuroImage* 31: 968–980, 2006.

27. **Destexhe A, Sejnowski T** *Thalamocortical Assemblies: How Ion Channels, Single Neurons and large-Scale Networks Organize Sleep Oscillations* Monographs of the Physiological Society. Oxford University Press, 2001.

28. **Destexhe A, Sejnowski TJ**. The Wilson–Cowan model, 36 years later. *Biological Cybernetics* 101: 1–2, 2009.

29. **Dudek FE**. Gap junctions and fast oscillations: A role in seizures and epileptogenesis? *Epilepsy Currents* 2: 133–136, 2002.

30. **Erlhagen W, Schoner G**. Dynamic field theory of movement preparation. *Psychological Reviews* 109: 545–572, 2002.

31. **Ermentrout B, Cowan JD**. Temporal oscillations in neuronal nets. *Journal of Mathematical Biology* 7: 265–80, 19879.

32. **Ermentrout GB, Cowan JD**. A mathematical theory of visual hallucination patterns. *Biological Cybernetics* 34: 137–150, 1979.

33. **Ermentrout GB, Cowan JD**. Large scale spatially organized activity in neural nets. *SIAM Journal on Applied Mathematics* 38, 1980.

34. **Feingold J, Gibson DJ, Pasquale BD, Graybiel AM**. Bursts of beta oscillation differentiate postperformance activity in the striatum and motor cortex of monkeys performing movement tasks. *Proceedings of the National Academy of Sciences* 112: 13687–13692, 2015.

35. **Forrester M, Coombes S, Crofts JJ, Sotiropoulos SN, O'Dea RD**. The role of node dynamics in shaping emergent functional connectivity patterns in the brain. *arXiv e-prints* p. arXiv:1906.11573, 2019.

36. **Fox MD, Buckner RL, White MP, Greicius MD, Pascual-Leone A**. Efficacy of transcranial magnetic stimulation targets for depression is related to intrinsic functional connectivity with the subgenual cingulate. *Biological Psychiatry* 72: 595–603, 2012.

37. **Fries P**. A mechanism for cognitive dynamics: Neuronal communication through neuronal coherence. *Trends in Cognitive Sciences* 9: 474–480, 2005.

38. **Fung P, Robinson P**. Neural field theory of synaptic metaplasticity with applications to theta burst stimulation. *Journal of Theoretical Biology* 340: 164–176, 2014.

39. **George MS, Nahas Z, Molloy M, Speer AM, Oliver NC, Li XB, Arana GW, Risch SC, Ballenger JC**. A controlled trial of daily left prefrontal cortex TMS for treating depression. *Biological Psychiatry* 48: 962–970, 2000.

40. **George MS, Wassermann EM, Williams WA, Callahan A, Ketter TA, Basser P, Hallett M, Post RM**. Daily repetitive transcranial magnetic stimulation (rTMS) improves mood in depression. *Neuroreport: An International Journal for the Rapid Communication of Research in Neuroscience* 2: 1853–1856, 1995.

41. **Gerfen CR, Economo MN, Chandrashekar J**. Long distance projections of cortical pyramidal neurons. *Journal of Neuroscience Research* 96: 1467–1475, 2018.

42. **Glasser MF, Sotiropoulos SN, Wilson JA, Coalson TS, Fischl B, Andersson JL, Xu J, Jbabdi S, Webster M, Polimeni JR et al.** The minimal preprocessing pipelines for the human connectome project. *NeuroImage* 80: 105–124, 2013.

43. **Grimbert F, Faugeras O**. Bifurcation Analysis of Jansen's Neural Mass Model. *Neural Computation* 18: 3052–3068, 2006.

44. **Guo S, Yu Y, Zhang J, Feng J**. A reversal coarse-grained analysis with application to an altered functional circuit in depression. *Brain and Behavior* 3: 637–648, 2013.

45. **Hagmann P, Cammoun L, Gigandet X, Meuli R, Honey CJ, Weeden VJ**. Mapping the structural core of human cerebral cortex. *PLoS Biology* 6: e159, 2008.

46. **Hall SD, Stanford IM, Yamawaki N, McAllister CJ, Rönnqvist KC, Woodhall GL, Furlong PL**. The role of GABAergic modulation in motor function related neuronal network activity. *NeuroImage* 56: 1506–1510, 2011.

47. **Hellyer PJ, Jachs B, Clopath C, Leech R**. Local inhibitory plasticity tunes macroscopic brain dynamics and allows the emergence of functional brain networks. *NeuroImage* 124: 85–95, 2016.

48. **Hlinka J, Coombes S**. Using computational models to relate structural and functional brain connectivity. *European Journal of Neuroscience* 36: 2137–2145, 2012.

49. **Honey CJ, Kötter R, Breakspear M, Sporns O**. Network structure of cerebral cortex shapes functional connectivity on multiple time scales. *Proceedings of the National Academy of Sciences* 104: 10240–10245, 2007.

50. **Honey CJ, Thivierge JP, Sporns O**. Can structure predict function in the human brain? *NeuroImage* 52: 766–776, 2010.

51. **Honey C, Sporns O, Cammoun L, Gigandet X, Thiran JP, Meuli R, Hagmann P**. Predicting human resting-state functional connectivity from structural connectivity. *Proceedings of the National Academy of Sciences* 106: 2035–2040, 2009.

52. **Hormuzdi SG, Filippov MA, Mitropoulou G, Monyer H, Bruzzone R**. Electrical synapses: a dynamic signaling system that shapes the activity of neuronal networks. *Biochimica et Biophysica Acta* 1662: 113–137, 2004.

53. **Horn DI, Yu C, Steiner J, Buchmann J, Kaufmann J, Osoba A, Eckert U, Zierhut K, Schiltz K, He H, Biswal B, Bogerts B, Walter M**. Glutamatergic and resting-state functional connectivity correlates of severity in major depression–the role of pregenual anterior cingulate cortex and anterior insula. *Frontiers in Systems Neuroscience* 4: 33, 2010.

54. **Iwabuchi SJ, Peng D, Fang Y, Jiang K, Liddle EB, Liddle PF, Palaniyappan L**. Alterations in effective connectivity anchored on the insula in major depressive disorder. *European Neuropsychopharmacology* 24: 1784–1792, 2014.

55. **Iwabuchi SJ, Raschke F, Auer DP, Liddle PF, Lankappa ST, Palaniyappan L**. Targeted transcranial theta-burst stimulation alters fronto-insular network and prefrontal GABA. *NeuroImage* 146: 395–403, 2017.

56. **Jaccard P**. The distribution of the flora in the alpine zone. 1. *New Phytologist* 11: 37–50, 1912.

57. **Jansen BH, Rit VG**. Electroencephalogram and visual evoked potential generation in a mathematical model of coupled cortical columns. *Biological Cybernetics* 73: 357–366, 1995a.

58. **Jansen BH, Rit VG**. Electroencephalogram and visual evoked potential generation in a mathematical model of coupled cortical columns. *Biological Cybernetics* 73: 357–366, 1995b.

59. **Jbabdi S, Sotiropoulos SN, Savio AM, Graña M, Behrens TE**. Model-based analysis of multishell diffusion MR data for tractography: How to get over fitting problems. *Magnetic resonance in medicine* 68: 1846–1855, 2012.

60. **Jirsa VK, Haken H**. A derivation of a macroscopic field theory of the brain from the quasi-microscopic neural dynamics. *Physica D* 99: 503–526, 1997.

61. **Kilpatrick ZP**. Synaptic mechanisms of interference in working memory. *Scientific Reports* 8: 7879, 2018.

62. **Kilpatrick ZP, Bressloff PC**. Effects of synaptic depression and adaptation on spatiotemporal dynamics of an excitatory neuronal network. *Physica D* 239: 547–560, 2010.

63. **Kolbinger HM, Höflich G, Hufnagel A, Müller HJ, Kasper S**. Transcranial magnetic stimulation (TMS) in the treatment of major depression — a pilot study. *Human Psychopharmacology: Clinical and Experimental* 10: 305–310, 1995.

64. **l Nunez P** *Neocortical Dynamics and Human EEG Rhythms* Oxford University Press, 1995.

65. **Laing CR**. Exact neural fields incorporating gap junctions. *SIAM Journal on Applied Dynamical Systems* 14: 1899–1929, 2015.

66. **Lan MJ, Chhetry BT, Liston C, Mann JJ, Dubin M**. Transcranial magnetic stimulation of left dorsolateral prefrontal cortex induces brain morphological changes in regions associated with a treatment resistant major depressive episode: An exploratory analysis. *Brain Stimulation* 9: 577–583, 2016.

67. **Lang N, Siebner HR, Chadaide Z, Boros K, Nitsche MA, Rothwell JC, Paulus W, Antal A**. Bidirectional modulation of primary visual cortex excitability: a combined tDCS and rTMS study. *Investigative Ophthalmology & Visual Science* 48: 5782–5787, 2007.

68. **Lea-Carnall CA, Montemurro MA, Trujillo-Barreto NJ, Parkes LM, El-Deredy W**. Cortical resonance frequencies emerge from network size and connectivity. *PLoS Computational Biology* 12: 1–19, 2016.

69. **Lee SH, Kim W, Chung YC, Jung KH, Bahk WM, Jun TY, Kim KS, George MS, Chae JH**. A double blind study showing that two weeks of daily repetitive TMS over the left or right temporoparietal cortex reduces symptoms in patients with schizophrenia who are having treatment-refractory auditory hallucinations. *Neuroscience Letters* 376: 177–181, 2005.

70. **Lett TA, Voineskos AN, Kennedy JL, Levine B, Daskalakis ZJ**. Treating working memory deficits in schizophrenia: a review of the neurobiology. *Biological Psychiatry* 75: 361–370, 2014.

71. **Liley DTJ, Cadusch PJ, Dafilis MP**. A spatially continuous mean field theory of electrocortical activity. *Network* 13: 67–113, 2002.

72. **Liu Z, Xu C, Xu Y, Wang Y, Zhao B, Lv Y, Cao X, Zhang K, Du C**. Decreased regional homogeneity in insula and cerebellum: a resting-state fMRI study in patients with major depression and subjects at high risk for major depression. *Psychiatry Research: Neuroimaging* 182: 211–215, 2010.

73. **Loo CK, Mitchell PB**. A review of the efficacy of transcranial magnetic stimulation (TMS) treatment for depression, and current and future strategies to optimize efficacy. *Journal of Affective Disorders* 88: 255–267, 2005.

74. **Lopes da Silva F**. EEG and MEG: relevance to neuroscience. *Neuron* 80: 1112–28, 2013.

75. **Lubenov EV, Siapas AG**. Decoupling through synchrony in neuronal circuits with propagation delays. *Neuron* 58: 118–131, 2008.

76. **Luke TB, Barreto E, So P**. Complete classification of the macroscopic behaviour of a heterogeneous network of theta neurons. *Neural Computation* 25: 3207–3234, 2013.

77. **Lundqvist M, Rose J, Herman P, Brincat SL, Buschman TJ, Miller EK**. Gamma and beta bursts underlie working memory. *Neuron* 90: 152–164, 2016.

78. **Martinet LE, Fiddyment G, Madsen JR, Eskandar EN, Truccolo W, Eden UT, Cash S, Kramer MA**. Human seizures couple across spatial scales through travelling wave dynamics. *Nature Communications* 8: 14896, 2017.

79. **Mayberg HS**. Limbic-cortical dysregulation: a proposed model of depression. *The Journal of Neuropsychiatry and Clinical Neurosciences* 9: 471–481, 1997.

80. **Meijer HGE, Eissa TL, Kiewiet B, Neuman JF, Schevon CA, Emerson RG, Goodman RR, McKhann GM, Marcuccilli CJ, Tryba AK, Cowan JD, van Gils SA, van Drongelen W**. Modeling focal epileptic activity in the Wilson–Cowan model with depolarization block. *The Journal of Mathematical Neuroscience* 5: 7, 2015.

81. **Menon V**. Large-scale brain networks and psychopathology: a unifying triple network model. *Trends in Cognitive Sciences* 15: 483–506, 2011.

82. **Menon V, Uddin LQ**. Saliency, switching, attention and control: a network model of insula function. *Brain Structure and Function* 214: 655–667, 2010.

83. **Mi Y, Lin X, Wu S**. Neural computations in a dynamical system with multiple time scales. *Frontiers in Computational Neuroscience* 10: 96, 2016.

84. **Montbrió E, Pazó D, Roxin A**. Macroscopic description for networks of spiking neurons. *Physical Review X* 5: 021028, 2015.

85. **Mormann F, Lehnertz K, David P, Elger CE**. Mean phase coherence as a measure for phase synchronization and its application to the EEG of epilepsy patients. *Physica D* 144: 358–369, 2000.

86. **Mountcastle VB**. The columnar organization of the neocortex. *Brain* 120: 701–722, 1997.

87. **Muller L, Chavane F, Reynolds J, Sejnowski TJ**. Cortical travelling waves: mechanisms and computational principles. *Nature Reviews Neuroscience* 19: 255–268, 2018.

88. **Newman MEJ** 2016 *Mathematics of Networks*, p. 1–8 Palgrave Macmillan UK, London.

89. **Noda Y, Silverstein WK, Barr MS, Vila-Rodriguez F, Downar J, Rajji TK, Fitzgerald PB, Mulsant BH, Vigod SN, Daskalakis ZJ, Blumberger DM**. Neurobiological mechanisms of repetitive transcranial magnetic stimulation of the dorsolateral prefrontal cortex in depression: A systematic review. *Psychological Medicine* 45: 3411–3432, 2015.

90. **Nunez PL**. The brain wave equation: a model for the EEG. *Mathematical Biosciences* 21: 279–297, 1974.

91. **Onslow ACE, Jones MW, Bogacz R**. A canonical circuit for generating phase-amplitude coupling. *PLoS ONE* 9: 1–15, 2014.

92. **Park HJ, Friston K**. Structural and functional brain networks: from connections to cognition. *Science* 342: 1238411, 2013.

93. **Pasley BN, Allen EA, Freeman RD**. State-dependent variability of neuronal responses to transcranial magnetic stimulation of the visual cortex. *Neuron* 62: 291–303, 2009.

94. **Peraza LR, Cromarty R, Kobeleva X, Firbank MJ, Killen A, Graziadio S, Thomas AJ, O'Brien JT, Taylor JP**. Electroencephalographic derived network differences in Lewy body dementia compared to Alzheimer's disease patients. *Scientific Reports* 8: 4637, 2018.

95. **Pfurtscheller G**, EEG event-related desynchronization (ERD) and event-related synchronization (ERS) In: *Electroencephalography. Basic Principles, Clinical Applications, and Related Fields*, edited by Niedermeyer E, da Silva FHL. Lippincott Williams and Wilkins, Baltimore, 4th edition, 4th edition, 1999 chapter 53, p. 958–967.

96. **Pyle R, Rosenbaum R**. Spatiotemporal dynamics and reliable computations in recurrent spiking neural networks. *Physical Review Letters* 118: 018103, 2017.

97. **Roberts JA, Gollo LL, Abeysuriya RG, Roberts G, Mitchell PB, Woolrich MW, Breakspear M**. Metastable brain waves. *Nature Communications* 10: 1–17, 2019.

98. **Robinson PA**. Neural field theory of synaptic plasticity. *Journal of Theoretical Biology* 285: 156–163, 2011.

99. **Robson SE, Brookes MJ, Hall EL, Palaniyappan L, Kumar J, Skelton M, Christodoulou NG, Qureshi A, Jan F, Katshu MZ, Liddle EB, Liddle PF, Morris PG**. Abnormal visuomotor processing in schizophrenia. *NeuroImage: Clinical* 12: 869–878, 2016.

100. **Rosenbaum R, Doiron B**. Balanced networks of spiking neurons with spatially dependent recurrent connections. *Physical Review X* 4: 021039, 2014.

101. **Rothkegel H, Sommer M, Paulus W, Lang N**. Impact of pulse duration in single pulse tms. *Clinical Neurophysiology* 121: 1915–1921, 2010.

102. **Rubinov M, Sporns O**. Complex network measures of brain connectivity: Uses and interpretations. *NeuroImage* 52: 1059–1069, 2010.

103. **Rubinov M, Sporns O, van Leeuwen C, Breakspear M**. Symbiotic relationship between brain structure and dynamics. *BMC Neuroscience* 10: 55, 2009.

104. **Rusu CV, Murakami M, Ziemann U, Triesch J**. A model of TMS-induced I-waves in motor cortex. *Brain Stimulation* 7: 401–414, 2014.

105. **Sanz-Leon P, Knock SA, Spiegler A, Jirsa VK**. Mathematical framework for large-scale brain network modeling in The Virtual Brain. *NeuroImage* 111: 385–430, 2015.

106. **Schevon CA, Weiss SA, McKhann Jr G, Goodman RR, Yuste R, Emerson RG, Trevelyan AJ**. Evidence of an inhibitory restraint of seizure activity in humans. *Nature Communications* 3: 1060, 2012.

107. **Schulz JB, Hausmann L, Hardy J**. 199 years of parkinson disease – what have we learned and what is the path to the future? *Journal of Neurochemistry* 139: 3–7, 2016.

108. **Sherman MA, Lee S, Law R, Haegens S, Thorn CA, Hämäläinen MS, Moore CI, Jones SR**. Neural mechanisms of transient neocortical beta rhythms: Converging evidence from humans, computational modeling, monkeys, and mice. *Proceedings of the National Academy of Sciences* 113: E4885–E4894, 2016.

109. **Shimamoto H, Morimitsu H, Sugita S, Nakahara K, Shigemori M**. Therapeutic effect of repetitive transcranial magnetic stimulation in Parkinson's disease. *Rinsho Shinkeigaku* 39: 1264–1267, 1999.

110. **Shusterman V, Troy WC**. From baseline to epileptiform activity: a path to synchronized rhythmicity in large-scale neural networks. *Physical Review E* 77: 061911, 2008.

111. **Siebner HR, Hartwigsen G, Kassuba T, Rothwell JC**. How does transcranial magnetic stimulation modify neuronal activity in the brain? Implications for studies of cognition. *Cortex* 45: 1035–1042, 2009.

112. **Sotiropoulos SN, Hernández-Fernández M, Vu AT, Andersson JL, Moeller S, Yacoub E, Lenglet C, Ugurbil K, Behrens TE, Jbabdi S**. Fusion in diffusion MRI for improved fibre orientation estimation: An application to the 3T and 7T data of the Human Connectome Project. *NeuroImage* 134: 396–409, 2016.

113. **Sridharan D, Levitin DJ, Menon V**. A critical role for the right fronto-insular cortex in switching between central-executive and default-mode networks. *Proceedings of the National Academy of Sciences* 105: 12569–12574, 2008.

114. **Stam C, van Straaten E, Van Dellen E, Tewarie P, Gong G, Hillebrand A, Meier J, Van Mieghem P**. The relation between structural and functional connectivity patterns in complex brain networks. *International Journal of Psychophysiology* 103: 149–160, 2016.

115. **Stancák A, Pfurtscheller G**. Desynchronization and recovery of β rhythms during brisk and slow self-paced finger movements in man. *Neuroscience Letters* 196: 21–24, 1995.

116. **Tewarie P, Hunt BAE, O'Neill GC, Byrne Á, Aquino K, Bauer M, Mullinger KJ, Coombes S, Brookes MJ**. Relationships between neuronal oscillatory amplitude and dynamic functional connectivity. *Cerebral Cortex* 29: 2668–2681, 2018.

117. **Thomas Yeo B, Krienen FM, Sepulcre J, Sabuncu MR, Lashkari D, Hollinshead M, Roffman JL, Smoller JW, Zöllei L, Polimeni, Polimeni JR, Fischl B, Liu H, Buckner RL**. The organization of the human cerebral cortex estimated by intrinsic functional connectivity. *Journal of Neurophysiology* 106: 1125–1165, 2011.

118. **Tik M, Hoffmann A, Sladky R, Tomova L, Hummer A, de Lara LN, Bukowski H, Pripfl J, Biswal B, Lamm C, Windischberger C**. Towards understanding rTMS mechanism of action: stimulation of the DLPFC causes network-specific increase in functional connectivity. *NeuroImage* 162: 289–296, 2017.

119. **Touboul J, Wendling F, Chauvel P, Faugeras O**. Neural mass activity, bifurcations, and epilepsy. *Neural Computation* 23: 3232–86, 2011.

120. **Valdes-Sosa PA, Sanchez-Bornot JM, Sotero RC, Iturria-Medina Y, Aleman-Gomez Y, Bosch-Bayard J, Carbonell F, Ozaki T**. Model driven EEG/fMRI fusion of brain oscillations. *Human Brain Mapping* 30: 2701–21, 2009.

121. **Van Den Heuvel MP, Pol HEH**. Exploring the brain network: a review on resting-state fMRI functional connectivity. *European Neuropsychopharmacology* 20: 519–534, 2010.

122. **Van Essen DC, Smith SM, Barch DM, Behrens TE, Yacoub E, Ugurbil K, Consortium WMH et al.** The WU-Minn human connectome project: an overview. *NeuroImage* 80: 62–79, 2013.

123. **van Straaten EC, Stam CJ**. Structure out of chaos: functional brain network analysis with EEG, MEG, and functional MRI. *European Neuropsychopharmacology* 23: 7–18, 2013.

124. **Velazquez JLP, Carlen PL**. Gap junctions, synchrony and seizures. *Trends in Neurosciences* 23: 68–74, 2000.

125. **Visser S, Nicks R, Faugeras O, Coombes S**. Standing and travelling waves in a spherical brain model: the Nunez model revisited. *Physica D* 349: 27–45, 2017.

126. **Vogels TP, Sprekeler H, Zenke F, Clopath C, Gerstner W**. Inhibitory plasticity balances excitation and inhibition in sensory pathways and memory networks. *Science* 334: 1569–1573, 2011.

127. **Wang XJ, Kennedy H**. Brain structure and dynamics across scales: in search of rules. *Current Opinion in Neurobiology* 37: 92–98, 2016.

128. **Wendling F, Bartolomei F, Bellanger J, Chauvel P**. Interpretation of interdependencies in epileptic signals using a macroscopic physiological model of the EEG. *Clinical Neurophysiology* 112: 1201–1218, 2001.

129. **Wilson HR, Blake R, Lee SH**. Dynamics of travelling waves in visual perception. *Nature* 412: 907–910, 2001.

130. **Wilson HR, Cowan JD**. Excitatory and inhibitory interactions in localized populations of model neurons. *Biophysical Journal* 12: 1–24, 1972.

131. **Wilson HR, Cowan JD**. A mathematical theory of the functional dynamics of cortical and thalamic nervous tissue. *Biological Cybernetics* 13: 55–80, 1973.

132. **Wu JY, Huang X, Zhang C**. Propagating waves of activity in the neocortex: What they are, what they do. *The Neuroscientist* 14: 487–502, 2008.

133. **Xia M, Wang J, He Y**. Brainnet viewer: a network visualization tool for human brain connectomics. *PloS ONE* 8: e68910, 2013.

134. **Zetterberg LH, Kristiansson L, Mossberg K**. Performance of a model for a local neuron population. *Biological Cybernetics* 31: 15–26, 1978.

135. **Zucker RS, Regehr WG**. Short-term synaptic plasticit. *Annual Review of Physiology* 64: 355–405, 2002.